UCSF

UC San Francisco Previously Published Works

Title

Infrared Methods for Assessment of the Activity of Natural Enamel Caries Lesions

Permalink

https://escholarship.org/uc/item/7dz2c5xj

Journal

IEEE Journal of Selected Topics in Quantum Electronics, 22(3)

ISSN

1077-260X

Authors

Lee, Robert C

Staninec, Michal

Le, Oanh

et al.

Publication Date

2016

DOI

10.1109/jstqe.2016.2542481

Peer reviewed

eScholarship.org Powered by the California Digital Library
University of California

Author Manuscript

Author Manuscript

Author Manuscript

Author Manuscript

HHS Public Access

Author manuscript

IEEE J Sel Top Quantum Electron. Author manuscript; available in PMC 2017 May 01.

Published in final edited form as:

IEEE J Sel Top Quantum Electron. 2016 ; 22(3): . doi:10.1109/JSTQE.2016.2542481.

Infrared Methods for Assessment of the Activity of Natural Enamel Caries Lesions

Robert C. Lee, **Michal Staninec**, **Oanh Le**, and **Daniel Fried**

Division of Biomaterials and Bioengineering, Department of Preventative and Restorative Dental Sciences, San Francisco School of Dentistry, University of California, San Francisco, CA 94143-0758 USA

Robert C. Lee: robert.lee@ucsf.edu; Michal Staninec: michal.staninec@ucsf.edu; Oanh Le: oanh.le@ucsf.edu; Daniel Fried: daniel.fried@ucsf.edu

Abstract

New diagnostic methods are needed for the accurate assessment of caries lesion activity to establish the need for surgical treatment. Detection of the highly mineralized surface layer that forms near the surface of the lesions as a result of remineralization is important for diagnosis of the lesion activity. Previous studies have demonstrated that novel imaging methods can be used to detect remineralization of artificial enamel caries lesions. In this paper, the activity of natural enamel caries lesions was assessed in-vitro via detection of the surface layer with PS-OCT and dehydration rate measurements with NIR reflectance and thermal imaging modalities. An automated approach for detecting the surface layer with PS-OCT yielded high sensitivity (= 0.79) and high specificity (= 0.93) with moderate correlation (R^2 = 0.5920) with histology. Significant differences in dehydration rate measurements were found between the active and the arrested lesions using both the NIR reflectance and thermal imaging modalities. These results demonstrate that these novel imaging methods are ideally suited for nondestructive, noninvasive and quantitative measurement of lesion activity during a single clinical examination in real-time.

Index Terms

Dental Caries; Enamel; Polarization-sensitive optical coherence tomography (PS-OCT); Near-infrared imaging; Remineralization

I. Introduction

NEW diagnostic methods are needed for the accurate assessment of caries lesion activity to establish the need for surgical treatment. It is well known that remineralization therapy via fluoride produces fluorapatite crystals that are much more resistant to acid challenge than the original hydroxyapatite of tooth enamel and dentin [1]. With a thick enough fluorapatite-rich surface layer, diffusion of calcium and phosphate ions at the lesion body, can be dramatically reduced [2–4]. This leads to the arrest of lesion progression and no further intervention is necessary. The surface layer of a lesion is important for diagnosis of the current “state of the lesion”, i.e., whether or not the caries lesion is active and expanding or whether the lesion has been arrested and is undergoing remineralization. Therefore, one cannot overstate the importance of accurate diagnosis of the lesion activity in its early stage

Author Manuscript Author Manuscript Author Manuscript Author Manuscript

of development at which point non-invasive preventive measures can be taken to halt further decay. It is advantageous to assess lesion activity using a nondestructive, noninvasive and quantitative method during a single clinical examination.

Current methods for lesion assessment are composed of a combination of visual and tactile exams, which are prone to subjective bias, interference from staining, are limited to exposed surfaces and there is the potential for permanent damage to the intact lesion surface layer from sharp instruments [5, 6]. In addition, the remineralized caries lesion still retains the white coloration due to the subsurface demineralization, which may lead to an inconclusive diagnosis of caries lesion activity [6]. The histological analyses for lesion assessment such as transverse microradiography (TMR) and polarized light microscopy (PLM) require destruction of the tooth, making both methods unsuitable for use *in-vivo*. Ekstrand et al. reported that it is extremely difficult to differentiate active lesions from inactive lesions in a single clinical examination without training or calibration [7]. Clinical criteria for caries lesion activity has been introduced by Nyvad et al. and incorporated by the ICDAS II caries classification system, but both also utilize visual-tactile examination [8, 9]. At advanced stages of caries, the surface of the lesion becomes further demineralized giving it chalky white surface appearance due to irregular surface erosion and cavitation [8, 10]. The arrested caries lesions exhibit a glossy appearance with a surface hardness that is comparable to sound enamel because they have a highly mineralized surface layer on the outer surface of the lesion [7, 8, 10]. Differences in surface porosity between arrested and active caries lesions may be discriminated using novel optical imaging methods.

Since optical diagnostic tools exploit changes in the light scattering of the lesion, they have great potential for the diagnosis of lesion activity. Optical coherence tomography (OCT) is a non-invasive technique for creating cross-sectional images of internal biological structures. Several studies both *in-vitro* and *in-vivo* have demonstrated that polarization-sensitive OCT (PS-OCT) is uniquely capable of this task since it provides a measurement of the reflectivity from each layer of the lesion and is able to show the formation of a zone of increased mineral density and reduced light scattering due to remineralization [11–14]. Polarization sensitivity is particularly valuable for resolving the structure of early caries lesions because caries lesions strongly scatter incident polarized light and the image in the cross-polarization axis to that of the incident polarization can provide improved lesion contrast. We have demonstrated in several studies that the lesion severity can be represented by the integrated reflectivity with depth in the CP-OCT image and the integrated reflectivity, ΔR, is analogous to the integrated mineral loss, ΔZ, obtained from TMR [15–18]. The presence of a surface zone of reduced light scattering in the OCT image may indicate the lesion is arrested. PS-OCT images are particularly valuable for resolving these highly mineralized surface layers since the image in the incident polarization shows the position of the tooth surface while the image in the cross-polarization shows the body of the subsurface lesion.

Recently, swept-source OCT (SS-OCT) systems have been introduced that are capable of operating at very high scan rates without a marked loss in the signal to noise ratio. Previous studies have shown that the high quality OCT images of caries lesions can be acquired using SS-OCT systems [19–21]. A combination of PS-OCT with SS-OCT (PS-SS-OCT) would allow rapid acquisition of high-resolution tomographic images in a clinical setting.

Author Manuscript Author Manuscript Author Manuscript Author Manuscript

In a previous PS-OCT study, we developed approaches to automatically detect the surface layer and measure its thickness with high accuracy in artificial enamel caries lesions [22]. Accurate detection and measurement of the transparent surface layer can provide extremely useful information about lesion activity. In this study, we evaluate whether PS-OCT coupled with the automated algorithm can be used to nondestructively measure these changes in the structure of natural occlusal and smooth surface enamel caries lesions.

As the lesion becomes arrested or undergoes remineralization, the permeability of the surface layer significantly decreases and the rate of water dehydration from the lesion depends on the lesion structure. The optical changes with water loss have been exploited via quantitative light-induced fluorescence (QLF), thermal imaging and near-infrared (NIR) imaging [23–26]. Kaneko et al. and Zakian et al. carried out caries detection studies with a thermal camera and an air-jet for evaporation on occlusal and smooth natural tooth surfaces [24, 25]. The endothermic behavior of the water evaporation causes a temperature decrease followed by a recovery to thermal equilibrium as the lesion becomes dry. Ando et al. reported that pulsed thermography is sensitive to the mineralization state of the tooth and has potential to be used for lesion activity assessment [27]. NIR imaging has also been exploited for caries detection since sound enamel is transparent in the NIR and the scattering coefficient increases exponentially with increasing mineral loss. Recent studies on NIR reflectance imaging with wavelengths coincident with high water absorption, at 1460 nm and beyond 1500 nm, demonstrated high lesion contrast for artificial and natural enamel caries lesions [28–30]. This suggests that changes in water content have a more profound effect on enamel transparency at NIR wavelengths than in the visible. In a previous study, we demonstrated that rate of water evaporation from artificial enamel lesions could be imaged with thermal and NIR reflectance imaging [31]. We also reported that the NIR reflectance imaging at wavelengths between 1400 nm and 1700 nm was capable of detecting significant differences between different periods of remineralization in artificial enamel lesions during the dehydration process [31]. The influence of hydration on enamel lesions can be investigated as an indirect indicator of the decreased permeability of water due to remineralization. In this study, we test the hypothesis that the thermal and NIR reflectance imaging methods can be used to selectively and accurately discriminate active natural enamel caries lesions from arrested natural enamel caries lesions and ultimately determine the caries lesion activity during the dehydration process.

II. Methods

A. Sample Selection and Examinations

Teeth extracted from patients in the San Francisco Bay area were collected, cleaned and sterilized with Gamma radiation. Sixty teeth with suspected enamel caries lesions were selected; lesions were identified as white or brown/black (pigmented spots) on the tooth surface. The teeth with an obvious cavitation to dentin and calculus were excluded from the study. The roots were cut off and the coronal portions of teeth were mounted on 1.2 cm × 1.2 cm × 3 cm delrin blocks.

Prior to the study, two clinicians that had been extensively trained and calibrated through practical exercises independently examined the teeth with 2.5× magnifying surgical loupes

Author Manuscript Author Manuscript Author Manuscript Author Manuscript

and a ball ended periodontal probe to gently check for loss of tooth structure and surface texture without damaging the tooth structure. Teeth were scored according to both the ICDAS II lesion classification and the ICDAS II lesion activity assessment criteria [9]. A total of 42 teeth were mutually classified with ICDAS II scores of 1, 2 and 3 by the two examiners and there were 22 smooth surface and 20 occlusal pits and fissure caries lesions. The two examiners subsequently used the ICDAS II lesion activity assessment criteria for determining the activity of the suspected lesions; the ICDAS II lesion activity assessment criteria utilizes color (white-black), luster (dull-shiny) and texture (smooth-rough) before and after 5 seconds of air-drying [9].

B. PS-OCT System

The PS-OCT system used in this study has been described previously [12]. An all fiber-based Optical Coherence Domain Reflectometry (OCDR) system with polarization maintaining (PM) optical fiber, high speed piezoelectric fiber-stretchers and two balanced InGaAs receivers that was designed and fabricated by Optiphase, Inc., Van Nuys, CA was used to acquire the images [32]. This two-channel system was integrated with a broadband superluminescent diode (SLD) DL-CS3159A, Denselight (Jessup, MD) and a high-speed XY-scanning motion controller system, ESP 300 controller with ILS100PP and 850G-HS stages, (Newport, Irvine, CA) for *in-vitro* optical tomography. A high power (15 mW) polarized SLD source operated at a center wavelength of 1317 nm with a spectral bandwidth full-width-half-maximum (FWHM) of 84 nm was used to provide an axial resolution of 9 μm in air and 6 μm in enamel (refractive index = 1.6). Light from the sample arm was focused onto the sample surface using a 20 mm focal length plano-convex lens providing a lateral resolution of approximately 20 μm.

The PS-OCT system was completely controlled using LabView™ software (National Instruments, Austin, TX). Samples were dried with pressurized air for 30 seconds prior to scanning. The A-scan sweep rate was 150 Hz with a dynamic range of 48 dB. Each A-scan was an average of 10 raw A-scans and was spaced 50 μm apart. The total number of data points in each A-scan was 2000 over a scan range of approximately 5 mm in air.

C. Calculation of Transparent Surface Layer Thickness, Lesion Depth and Integrated Reflectivity (ΔR)

PS-OCT images were processed using a dedicated program constructed with LabView™ software. There was a phase shift in the PM-fiber between the two axes, so an axial position calibration was performed once prior to the study. A gold mirror was scanned at a 150 Hz sweep rate and each A-scan was an average of 100 scans. Five hundred A-scans were acquired at 10 μm intervals over the entire scan range to determine the required axial position adjustments and the axial position of the cross-polarization scan images was adjusted to match the co-polarization scan images.

The position of the strong surface reflection in the co-polarization axis and the strong scattering of polarized light from the underlying lesion body in the cross-polarization axis were used to measure the thickness of the transparent surface layer. Surface layer detection and measurement utilized an edge detection technique using the zero-crossing first-order

Author Manuscript Author Manuscript Author Manuscript Author Manuscript

derivative as described previously [22, 33]. Binary images were generated to indicate either the presence or absence of the transparent surface layer and a 5×5 morphological closing operation with a 50% threshold was subsequently applied to the binary images in order to reduce false-negatives [22]. Pixels were converted to microns in enamel using a refractive index correction of 1.6 to yield the final transparent surface layer thickness.

The lesion depth was calculated using a previously developed algorithm [22]. An edge locator was used to make two passes along each A-scan of the processed CP-OCT images to locate the respective positions at which the intensity has decreased to half of the lesion peak maximum. A linear relationship was established between the lesion depth using PS-OCT and the histological lesion depths measured using polarized light microscopy (PLM) [22, 34].

Previous studies have shown that the integrated reflectivity, ΔR, over the estimated lesion depth positively correlates with the integrated mineral loss (volume percent mineral loss × μm), ΔZ [16, 17]. ΔR was calculated by integrating from the base of the transparent layer through the entire estimated lesion body in the CP-OCT images [22]. This had the added advantage of removing the contribution of the high specular reflection at the surface of the transparent layer, which was large enough to be present even in the CP-OCT images. A 5 × 5 pixel median filter was applied to the final 2D projection images for improved visualization.

D. Dehydration Measurements

The following setup was used for the dehydration experiments of sec. E and F. Each sample was placed in a mount connected to a high-speed XY-scanning motion controller system, Newport ESP 300 controller & 850G-HS stages coupled with air nozzles connected together to a compressed air and a light source [31]. Each sample was immersed in the water bath for 60 seconds while being vigorously shaken to enhance water diffusion. After the sample was removed from the water bath, the excess water on the surface of the lesion with a disposable cotton roll. An image was captured as an initial reference image and the air spray was activated. Seven air nozzles were positioned 5 cm away from sample and the air pressure was set to 12 psi. Each measurement consisted of capturing a sequence of images at 4 frames per second for 60 seconds. The air nozzles and the light source were centered on the suspected lesion. The dehydration setup was completely automated using LabView™.

E. Thermal Imaging and Analysis

A Model A65 infrared (IR) thermography camera (FLIR Systems, Wilsonville, OR) sensitive from 7.5 – 13 μm with a resolution of 640 × 512 pixels, a thermal sensitivity of 50 mK and a lens with a 13 mm focal length was used to record temperature changes during the dehydration process. The area per pixel was approximately 0.02 mm^2. The ambient room temperature, flowing air temperature and water bath temperature were approximately 21 °C (294.15 K) and were consistent throughout the experiment. The object emissivity was set to 0.91, and the atmospheric temperature was set to 294.15 K [35]. Relative humidity was set at a default value of 50%; humidity values were not recorded, but every sample was measured under the same conditions. Previous studies have shown that ΔQ, the area enclosed by the

Author Manuscript Author Manuscript Author Manuscript Author Manuscript

time-temperature curve, can be used as a quantitative measure of porosity and can be used to discriminate between sound and demineralized enamel *in-vitro* [24].

Thermal images were processed and analyzed using a dedicated program written in Labview™. The thermography camera outputs a series of temperature measurements over time. The initial reference temperature measurements varied slightly (± 0.5 K) due to variations in emissivity, lesion structure, mineral composition and water content among windows. Calibration was carried out via matching the measurements from the initial reference image to the ambient temperature. ΔQ was calculated from the area enclosed by the initial temperature and the time-temperature curve.

F. NIR Reflectance Imaging and Analysis

An Indigo Alpha NIR camera (FLIR Systems, Wilsonville, OR) with an InGaAs focal plane array, a spectral sensitivity range from 900 nm to 1750 nm, a resolution of 320 × 256 pixels and an InfiniMite™ lens (Infinity, Boulder, CO) was used to acquire all the images during the dehydration process. The area per pixel was approximately 0.003 mm^2. Light from a 150 W fiber-optic illuminator FOI-1 (E Licht Company, Denver, CO) was directed at the sample with crossed polarizers and a long-pass filter at 1400 nm (1400 – 1700 nm). Source to sample distance was fixed at 5 cm for all samples.

NIR reflectance images were processed and automatically analyzed using a dedicated program constructed with LabView™ software. The intensity difference between the final and initial images, ΔI, was calculated using $I(t=60) - I_I$, where I(t=60) is the mean intensity at t = 60 seconds and I_I is the mean intensity prior to turning on the air nozzle.

In order to investigate the rate of intensity change in conjunction with the overall intensity change, the “S”-shaped time-intensity curve was fit to a sigmoid function previously described in Eq (2) in [31], and the overall growth rate (OGR) was calculated.

G. Polarized Light Microscopy (PLM), Transverse Microradiography (TMR) and Histological Validation of Lesion Activity

After sample imaging was completed, 200 μm thick serial sections were cut using an Isomet 5000 saw (Buehler, IL) for PLM and TMR. PLM was carried out using a Meiji Techno Model RZT microscope (Meiji Techno Co., LTD, Saitama, Japan) with an integrated digital camera, Canon EOS Digital Rebel XT (Canon Inc., Tokyo, Japan). The sample sections were imbibed in water and examined in the brightfield mode with crossed polarizers and a red I plate with 500 nm retardation. PLM images were acquired at 35× magnification and had a resolution of 3264 × 2448 pixels.

A custom built digital microradiography (TMR) system was used to detect the surface zone of the increased mineral content on the tooth sections [36]. High-resolution microradiographs were taken using Cu Kα radiation from a Philips 3100 X-ray generator and a Photonics Science FDI X-ray digital imager, Microphotonics (Allentown, PA). The X-ray digital imager consisted of a 1392×1040 pixel interline CCD directly bonded to a coherent micro fiber-optic coupler that transfers the light from an optimized gadolinium oxysulfide scintillator to the CCD sensor. The pixel resolution was 2.1 μm and the images

Author Manuscript Author Manuscript Author Manuscript Author Manuscript

were acquired at 10 frames per second. A high-speed motion control system with Newport UTM150 and 850G stages and an ESP 300 controller coupled to a video microscopy and a laser targeting system was used for precise positioning of the sample in the field of view of the imaging system.

For the histological validation of the lesion activity, changes in mineral content were measured with PLM and TMR. Arrested caries lesions have a distinct transparent surface layer with islands of negatively birefringent enamel within the positively birefringent body of the enamel in water [10]. Irregular surface defects such as cavitation were also recorded. The thickness of transparent surface layer was measured using the image analysis package incorporated in Igor Pro (Wavemetrics, Lake Oswego, OR). If a distinct transparent surface layer was found, the activity of the suspected caries lesion was categorized as “arrested”. If the lesion did not have a transparent surface layer or a discontinuity of the surface layer due to surface irregularities, the lesion activity was categorized as “active”.

H. Statistical Analysis

Sample groups were compared using analysis of variance (ANOVA) with a Tukey–Kramer post hoc multiple comparison test. Linear regression with Pearson’s correlation was used to examine the relationship between data acquired from PS-OCT and PLM measurements. Performances of the infrared imaging methods were evaluated using receiver operating characteristic (ROC) curves. All statistical analyses were performed with 95% confidence with Prism™ (GraphPad software, San Diego, CA).

III. Results

A. ICDAS II Lesion Activity Assessment

Two examiners relied on the ICDAS II lesion classification criteria for determining the stages of the caries process of the suspected natural caries lesion samples solely to screen teeth for lesion activity assessment. The ICDAS II scores ranged from 0 to 4 and a total of 42 teeth were mutually scored as 1, 2 and 3 by the two examiners. The inter-examiner agreement for ICDAS II lesion classification criteria was 81%, and kappa values were 0.594 (unweighted) and 0.620 (weighted).

For the activity of the smooth surface enamel caries lesion samples, the inter-examiner agreement was 95%; kappa values were not reported because kappa statistics is not reliable due to its limitations for skewed data sets. With the true-positive being the successful diagnosis of an active lesion based on histological findings, the two examiners yielded an average sensitivity of 0 and an average specificity of 0.97; one examiner diagnosed all lesions as arrested and another examiner diagnosed one lesion as an active lesion. Eighteen of the 22 smooth surface lesion samples exhibited the transparent surface layer with histology and were categorized as arrested caries lesions.

For the activity of the occusal pits and fissure caries lesion samples, the inter-examiner agreement was 45% with a kappa value of −0.06. The two examiners yielded an average sensitivity of 0.65 and an average specificity of 0.50. Ten of the 20 occlusal pits and fissure lesion samples exhibited a transparent surface layer in the center of pits and fissures with

Author Manuscript Author Manuscript Author Manuscript Author Manuscript

histology and were categorized as arrested caries lesions. Some samples exhibited the transparent surface layer on the smooth surface around pits and fissures but with distinct surface demineralization or micro-cavitation in the pits and fissures. Such samples were categorized as active lesions. When the two data sets were combined and analyzed, the inter-examiner agreement was 71% agreement of diagnoses with a kappa value of 0.32. The two examiners yielded an average sensitivity of 0.46 and an average specificity of 0.80 for all samples.

B. Infrared Imaging Methods for Lesion Activity Assessment

Arrested and active smooth surface enamel lesions are shown in Figs. 1 and 2, respectively, with the visible images (A), histology with PLM (B & C) and results from PS-OCT (D – F), thermal (G) and NIR reflectance (H & I) methods. PLM images of the arrested smooth surface enamel caries lesion (Figs. 1B & 1C) show a thin layer of the transparent surface layer above the subsurface lesion, and PS-OCT was able to estimate the severity and location of the subsurface lesion and accurately estimate the thickness of the transparent surface layer (Figs. 1D – 1F). The active smooth surface enamel caries lesions show microcavitation of the surface without a distinctive surface layer (Figs. 2B & 2C). The thermal imaging (Figs. 1G & 2G) and the NIR reflectance images (Figs. 1H – 1I & 2H – 2I) show significant differences in ΔQ, ΔI and OGR measurements in the suspected lesion area.

An arrested occlusal pit and fissure caries lesion is shown in Fig. 3 and an active occlusal caries lesion is shown in Fig. 4 with the visible images shown in (A), histology with PLM (B & C) and results from PS-OCT (D – F), thermal (G) and NIR reflectance (H & I) methods. PLM images of the arrested occlusal lesion (Figs. 3B & 3C) show a thin layer of the transparent surface layer above the subsurface lesion. However, Fig. 4 shows both active and arrested occlusal pits and fissure caries lesions in one sample; Fig. 4B shows demineralization of the surface structure with cavitation at pits and fissures, and Fig. 4C shows an arrested pit and fissure lesion with a distinct surface layer. PS-OCT was able to estimate the severity and location of the subsurface lesion and accurately estimate the thickness of the transparent surface layer (Figs. 3D – 3F & 4D – 4F). The thermal imaging (Figs. 3G & 4G) and the NIR reflectance images (Figs. 3H – 3I & 4H – 4I) show significant differences in ΔQ, ΔI and OGR measurements in the suspected lesion area.

In our previous study, the automated algorithm for detection and measurement of the transparent surface layer using PS-OCT proved to have high accuracy and high correlation with histology for the artificial enamel caries lesions [22]. In this study, PS-OCT accurately detected lesions without the transparent surface layer; PS-OCT yielded a sensitivity of 0.75 and a specificity of 0.94 for the smooth surface lesions, a sensitivity of 0.80 and a specificity of 0.90 for the occlusal pits and fissure lesions, and a sensitivity of 0.79 and a specificity of 0.93 for all lesions. For the all true-negative samples (n = 26), the thickness of the transparent surface layer estimated with PS-OCT showed a moderate correlation with the thickness measured with PLM as shown in Fig. 5 (Pearson's correlation, $p < 0.0001$, $R^2 = 0.5920$). There was a significant difference in the integrated reflectivity, ΔR, between active and arrested lesion groups of the pits and fissure caries lesion samples, but there was no

Author Manuscript Author Manuscript Author Manuscript Author Manuscript

significant difference between active and arrested lesion groups of the smooth surface caries lesion samples as shown in Table I.

It has been shown that the highly mineralized surface layer plays an important role in the dehydration process of remineralized artificial enamel lesions and both the thermal and NIR imaging methods are suitable for detection of remineralization in artificial enamel models [31]. All three methods, ΔQ, ΔI and OGR, showed a significant reduction in measurements with the presence of transparent surface layer ($P < 0.05$) as shown in Table 1, and these infrared imaging modalities showed strong performances in accurately diagnosing active lesions as indicated by the area under the curve from the ROC analysis, which are summarized in Table 2.

IV. Discussion

Detection of the highly mineralized surface layer that forms near the surface of the lesions as a result of remineralization is critical for the accurate diagnosis of lesion activity. The principal aim of this study was to demonstrate that the rate of water evaporation measured using thermal and NIR reflectance imaging methods could be used to assess the lesion activity of natural enamel caries lesions. A secondary aim of this study was to determine whether the automated transparent surface layer detection algorithm for PS-OCT could accurately detect and measure the thickness of the highly mineralized surface layer in natural enamel caries lesions.

There are significant challenges for the accurate diagnosis of caries lesion activity. Wenzel claimed that lesions confined to enamel might not be evident radiographically until there is approximately 30 – 40 % mineral loss [37]. Thus, radiographs are not suitable in lesion activity assessment of early caries lesions. Clinicians currently rely heavily on visual and tactile examination when a suspected lesion is not evident radiographically. Since conventional methods for diagnosis of lesion activity are highly subjective, rigorous training and calibration are required. Examiners in this study classified most of the smooth surface enamel lesions as arrested lesions and this caused a large discrepancy in sensitivity and specificity. In addition, the inter-examiner reliability was poor for the activity of the occlusal pits and fissure caries lesion samples, and the diagnostic performance of lesion activity assessment via ICDAS II guideline was also poor based on the low sensitivity and low specificity. This result suggests that clinicians cannot easily distinguish subtle tactile and visual changes in early enamel lesions and the subjectivity plays a large role with conventional diagnostic methods for lesion activity assessment. As reported in this study and another study by Ekstrand et al., the inter-examiner reproducibility was in general poor for the conventional lesion activity diagnostic methods [7]. Therefore, the ICDAS II training or score system was not accurate for assessing lesion activity in this study.

ICDAS II Lesion Activity Assessment criteria recommends that examiners use a ball-pointed probe with a diameter of 400 μm for tactile examination, but most pits and fissures are often too narrow for accurate lesion assessment [9]. The suspected caries lesion may contain microcavitations that are not visible to the naked eye, and this can further confound the conventional diagnostic approach.

Author Manuscript Author Manuscript Author Manuscript Author Manuscript

Conventional lesion activity assessment that relies on visual and tactile examination lacks certainty and reproducibility, and this study reinforces the importance of new methods with improved diagnostic performance. In a previous PS-OCT study, we demonstrated that an algorithm for automatic detection and measurement of the highly mineralized surface layer could be used on artificial enamel lesions with high accuracy and correlation [22]. When the algorithm was applied to the PS-OCT images for natural enamel caries lesions, higher sensitivity and specificity were achieved in determining enamel caries lesion activity compared to the conventional tactile and visual exams. In addition, thickness measurements of the highly mineralized surface layer showed strong correlation with histology indicating that PS-OCT could be used for estimating the degree of remineralization.

ICDAS II lesion activity assessment criteria provides a guideline in predicting lesion activity based on lesion location [9]. Ekstrand et al. classified cariogenic plaque stagnation areas (PSA) on different surfaces (occlusal, buccal, lingual and proximal surfaces) as an activity predictor [38]. Our results indicate that the majority of the natural enamel lesions are indeed found in PSA's, but the location of the lesion cannot be used as a sole predictor of lesion activity. For the occlusal pits and fissures lesions, visual and tactile examination is further challenged by the complex anatomy of the tooth. Ekstrand et al. stated that PSA's on occlusal surfaces depends on the size of the pits and fissures, i.e., pits and fissures greater than 400 μm were categorized as PSA's [38]. However, the histological analysis from this study showed multiple active caries lesions confined within the pits and fissures much smaller than 400 μm diameter.

Furthermore, there was a significant decrease in ΔR, integrated reflectivity, in the arrested lesion group of the pits and fissure caries lesions compared to all other groups as shown in Table I. All the arrested caries lesions found in the pits and fissures were incipient enamel caries lesions, which were confined within the outer half of enamel, and most of the active caries lesions in the pits and fissures presented with surface discontinuities. On the contrary, over 80 % of the smooth surface enamel lesions were categorized as arrested lesions.

In a previous study, we also reported that the highly mineralized surface layer plays an important role in the dehydration process and both the thermal and NIR reflectance imaging methods are suitable for detection of remineralization [31]. In this study, ΔQ, ΔI and OGR measurements were recorded and showed significant differences between active and arrested lesions. The results for smooth surface enamel caries were similar to the measurements from the previous artificial enamel caries lesion study as expected [31]. However, the occlusal caries lesions were mostly confined within the center of the pits and fissures and the differences in ΔQ, ΔI and OGR measurements between active and arrested lesions for the pits and fissure caries lesions were greater than those in the smooth surface enamel caries lesions. The anatomic structure of occlusal surface is complex; there are variations in the occlusal anatomy, the distance between surface to DEJ, and the orientation of enamel spindle among different dentition. We implemented seven air-jet nozzles in order to facilitate uniform pressurized air coverage and excess water was removed from the tooth surface with a cotton roll, water still accumulated within the pits and fissures extending the time for dehydration. Although we reported that thermal imaging showed a significant difference in detecting occlusal pits and fissures caries lesions from sound tissue as shown in Table I, the

Author Manuscript Author Manuscript Author Manuscript Author Manuscript

difference in ΔQ measurements between the sound pits and fissures and the sound smooth surface was large enough to cause false-positives as shown in Figs. 3G and 4G. Other factors such as differences in the heat dissipation of different materials and the presence of cracks may also influence ΔQ measurements. Zakian et al. reported that a larger ΔQ was observed at the cavity openings because the fissure pattern would be the principal escape route for water [25].

NIR reflectance imaging also suffered from similar problems during the dehydration process but to a lesser extent; the differences in ΔI and OGR measurements between the pits and fissure caries lesions and the smooth surface enamel caries lesions were smaller than ΔQ measurements. Although the complex anatomy of the occlusal surface also introduces challenges in NIR reflectance imaging including greater variation in the angle of incidence, surface scattering, and reflectivity, the NIR wavelengths utilized in this study are not adversely affected by heat dissipation problem found in ΔQ measurements. Thus, the NIR measurements are more localized and provide higher spatial resolution compared to thermal imaging. Our findings suggest that both the ΔI and OGR measurements provide useful information about the remineralization status of the lesion. In our previous study, we reported that OGR could be used to accentuate the active enamel lesions in artificial enamel model [31]. As shown in Figs. 2I and 4I, OGR shows the location of active enamel caries lesions with high contrast.

V. Conclusion

Our findings suggest that dehydration measurements with thermal and NIR reflectance imaging are suitable for assessment of enamel caries lesion activity. NIR reflectance imaging was the most effective and selective method in detecting active enamel caries lesions during the dehydration process. PS-OCT coupled with the automated algorithm was effective in detection and measurement of the highly mineralized surface layer in natural caries lesions. Images generated with PS-OCT provide useful information for estimating the severity and the degree of remineralization of the lesion. This study shows that the novel optical imaging methods are suitable for enamel caries lesion activity assessment in a single examination and that these imaging methods are superior in accuracy and selectivity in enamel caries lesion activity assessment compared to the conventional visual and tactile examination.

Acknowledgments

This work was supported in part by the National Institute of Health under Grants F30-DE023278, R01-DE17869 and R01-DE14698.

Biographies

Robert C. Lee received his D.D.S. degree from the University of California, San Francisco, CA, in 2013. He is currently working toward the Ph.D degree at the University of California, San Francisco.

Author Manuscript Author Manuscript Author Manuscript Author Manuscript

Michal Staninec received his D.D.S. degree from the University of California, Berkeley in 1980 and his Ph.D. degree from the University of Nijmegen, Holland in 1999.

He is currently a Health Sciences Clinical Professor, Emeritus in the Department of Preventative and Restorative Dental Sciences, University of California, San Francisco. He is also a practicing dentist and has been involved in studies of dental materials, caries detection, and the interaction of lasers with dental hard tissues.

Oanh Le received her D.D.S. degree from Northwestern University, Evanston, IL, in 1989. She earned a certificate in Advanced Education in General Dentistry from the University of California, San Francisco, CA, in 1992.

She is currently a Health Sciences Clinical Professor in the Department of Preventative and Restorative Dental Sciences, University of California, San Francisco. She is a practicing dentist and she has served as the chair for two terms of Consortium of Operative Dentistry Educators.

Daniel Fried received his Ph.D. degree in Physical Chemistry from Wayne State University, Detroit, MI in 1992.

He is currently a Professor in Division of Biomaterials and Bioengineering, Department of Preventative and Restorative Dental Sciences, University of California, San Francisco. He the has been involved in studies of caries detection, dental hard tissue optics, and the interaction of lasers with dental hard tissues since 1993 and he has published more than 200 original manuscripts in this area.

References

1. Kidd, EAM.; Joyston-Bechal, S. Dental Caries: The Disease and its Clinical Management. 3rd. Oxford University Press; 1997.
2. ten Cate JM, Featherstone JDB. Mechanistic aspects of the interactions between fluoride and dental enamel. Crit Rev Oral Biol Med. 1991; 2:283–296. [PubMed: 1892991]
3. ten Cate JM, Arends J. Remineralization of artificial enamel lesions in vitro. Caries Res. 1977; 11:277–86. [PubMed: 18285]
4. Kidd EA. The histopathology of enamel caries in young and old permanent teeth. British dental journal. Sep 24.1983 155:196–8. [PubMed: 6578821]
5. NIH. Diagnosis and Management of Dental Caries throughout Life. NIH Consensus Statement. Mar 26–28.2001 18 2001.
6. Ekstrand KR, Zero DT, Martignon S, Pitts NB. Lesion activity assessment. Monographs in oral science. 2009; 21:63–90. [PubMed: 19494676]
7. Ekstrand KR, Ricketts DN, Longbottom C, Pitts NB. Visual and tactile assessment of arrested initial enamel carious lesions: an in vivo pilot study. Caries Res. May-Jun;2005 39:173–7. [PubMed: 15914977]
8. Nyvad B, Machiulskiene V, Baelum V. Reliability of a new caries diagnostic system differentiating between active and inactive caries lesions. Caries Res. Jul-Aug;1999 33:252–60. [PubMed: 10343087]
9. Ismail, A.; Banting, D.; Eggertsson, H.; Ekstrand, K.; Ferreira-Zandona, A.; Longbottom, C., et al. In Proceedings of the 7th Indiana Conference. Indianapolis: Indiana University; 2005. Rationale and evidence for the International Caries Detection and Assessment System (ICDAS II); p. 161-221.

Author Manuscript Author Manuscript Author Manuscript Author Manuscript

10. Thylstrup A, Bruun C, Holmen L. In vivo caries models–mechanisms for caries initiation and arrestment. Adv Dent Res. Jul.1994 8:144–57. [PubMed: 7865069]
11. Amaechi BT, Higham SM, Podoleanu Ag, Rodgers JA, Jackson DA. Use of Optical Coherence Tomography for Assessment of Dental caries. J Oral Rehab. 2001; 28:1092–1093.
12. Fried D, Xie J, Shafi S, Featherstone JDB, Breunig T, Lee CQ. Early detection of dental caries and lesion progression with polarization sensitive optical coherence tomography. J Biomed Optics. 2002; 7:618–627.
13. Jones RS, Darling CL, Featherstone JDB, Fried D. Remineralization of in vitro Dental Caries Assessed with Polarization Sensitive Optical Coherence Tomography. J Biomed Opt. 2006; 11:014016. [PubMed: 16526893]
14. Louie T, Lee C, Hsu D, Hirasuna K, Manesh S, Staninec M, et al. Clinical assessment of early tooth demineralization using polarization sensitive optical coherence tomography. Lasers in Surg Med. 2010; 42:738–745. [PubMed: 21246578]
15. Chong SL, Darling CL, Fried D. Nondestructive measurement of the inhibition of demineralization on smooth surfaces using polarization-sensitive optical coherence tomography. Lasers in Surgery and Medicine. Jun.2007 39:422–7. [PubMed: 17565731]
16. Jones RS, Darling CL, Featherstone JD, Fried D. Imaging artificial caries on the occlusal surfaces with polarization-sensitive optical coherence tomography. Caries research. 2006; 40:81–89. [PubMed: 16508263]
17. Ngaotheppitak P, Darling CL, Fried D. Polarization Optical Coherence Tomography for the Measuring the Severity of Caries Lesions. Lasers Surg Med. 2005; 37:78–88. [PubMed: 15889402]
18. Arends J, Ruben JL, Inaba D. Major topics in quantitative microradiography of enamel and dentin: R parameter, mineral distribution visualization, and hyper-remineralization. Adv Dent Res. Nov. 1997 11:403–14. [PubMed: 9470497]
19. Shimada Y, Sadr A, Burrow MF, Tagami J, Ozawa N, Sumi Y. Validation of swept-source optical coherence tomography (SS-OCT) for the diagnosis of occlusal caries. J Dent. Aug.2010 38:655–65. [PubMed: 20470855]
20. Natsume Y, Nakashima S, Sadr A, Shimada Y, Tagami J, Sumi Y. Estimation of lesion progress in artificial root caries by swept source optical coherence tomography in comparison to transverse microradiography. J Biomed Opt. Jul.2011 16:071408. [PubMed: 21806254]
21. Nee A, Chan K, Kang H, Staninec M, Darling CL, Fried D. Longitudinal monitoring of demineralization peripheral to orthodontic brackets using cross polarization optical coherence tomography. J Dent. Feb 20.2014 42:547–555. [PubMed: 24561340]
22. Lee RC, Kang H, Darling CL, Fried D. Automated assessment of the remineralization of artificial enamel lesions with polarization-sensitive optical coherence tomography. Biomedical Optics Express. 2014; 5:2950–2962. 2014/09/01. [PubMed: 25401009]
23. Ando M, Stookey GK, Zero DT. Ability of quantitative light-induced fluorescence (QLF) to assess the activity of white spot lesions during dehydration. Am J Dent. Feb.2006 19:15–8. [PubMed: 16555651]
24. Kaneko, K.; Matsuyama, K.; Nakashima, S. Early detection of Dental caries II. Indianapolis, IN: 1999. Quantification of Early Carious Enamel Lesions by using an Infrared Camera; p. 83-99.
25. Zakian CM, Taylor AM, Ellwood RP, Pretty IA. Occlusal caries detection by using thermal imaging. Journal of Dentistry. 2010; 38:788–795. [PubMed: 20599464]
26. Usenik P, Bürmen M, Fidler A, Pernuš F, Likar B. Near-infrared hyperspectral imaging of water evaporation dynamics for early detection of incipient caries. Journal of Dentistry. 2014 In Press.
27. Ando M, Sharp N, Adams D. Pulse thermography for quantitative nondestructive evaluation of sound, de-mineralized and re-mineralized enamel. 2012:83480S-83480S-7.
28. Chung S, Fried D, Staninec M, Darling CL. Multispectral near-IR reflectance and transillumination imaging of teeth. Biomedical Optics Express. 2011; 2:2804–2814. [PubMed: 22025986]
29. Fried WA, Darling CL, Chan K, Fried D. High Contrast Reflectance Imaging of Simulated Lesions on Tooth Occlusal Surfaces at Near-IR Wavelengths. Lasers Surg Med. 2013; 45:533–541. [PubMed: 23857066]

Author Manuscript Author Manuscript Author Manuscript Author Manuscript

30. Simon JC, Chan KH, Darling CL, Fried D. Multispectral near-IR reflectance imaging of simulated early occlusal lesions: Variation of lesion contrast with lesion depth and severity. Lasers Surg Med. Mar.2014 46:203–215. [PubMed: 24375543]
31. Lee RC, Darling CL, Fried D. Assessment of remineralization via measurement of dehydration rates with thermal and near-IR reflectance imaging. J Dent. Apr 8.2015
32. Bush J, Davis P, Marcus MA. All-Fiber Optic Coherence Domain Interferometric Techniques. Fiber Optic Sensor Technology II. 2000:71–80.
33. Lee, RC.; Darling, CL.; Fried, D. Lasers in Dentistry X. San Jose: 2014. Automated detection of remineralization in simulated enamel lesions with PS-OCT; p. 1-8.
34. Chan KH, Chan AC, Fried WA, Simon JC, Darling CL, Fried D. Use of 2D images of depth and integrated reflectivity to represent the severity of demineralization in cross-polarization optical coherence tomography. J Biophotonics. 2015; 8:36–45. [PubMed: 24307350]
35. Lin M, Liu QD, Xu F, Bai BF, Lu TJ. In vitro investigation of heat transfer in human tooth. 2009:75222N-75222N-7.
36. Darling, CL.; Featherstone, JDB.; Le, CQ.; Fried, D. Lasers in Dentistry VX. San Jose: 2009. An automated digital microradiography system for assessing tooth demineralization; p. 1-7.
37. Wenzel, A. Dental Caries. In: White, SC.; Pharoah, MJ., editors. Oral radiology: principles and interpretation. UK, PA: Mosby Elsevier; 2008. p. 270-281.
38. Ekstrand KR, Martignon S, Ricketts DJ, Qvist V. Detection and activity assessment of primary coronal caries lesions: a methodologic study. Oper Dent. May-Jun;2007 32:225–35. [PubMed: 17555173]

Author Manuscript Author Manuscript Author Manuscript Author Manuscript

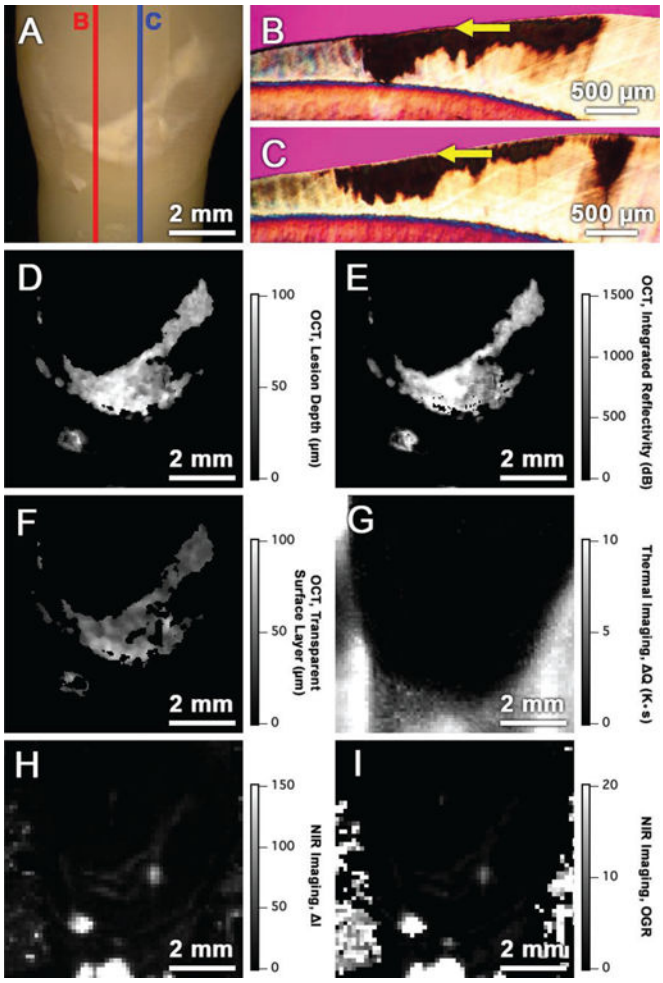

Fig. 1.

Visible, cross-sectional PLM, PS-OCT, thermal, and NIR reflectance images of an arrested smooth surface enamel caries lesion. The red line in the visible light reflectance image (A) represents the position of the PLM section shown in (B) and the blue line represents the position of the PLM section shown in (C). Lesion depths (D), lesion severity, estimated with integrated reflectivity (E), and transparent surface layer thickness (F) measurements with PS-OCT correlate well with histology (B and C). ΔQ (G) measurements with thermal imaging and ΔI (H) and OGR (I) measurements with NIR imaging show the suspected lesion. Yellow arrows designate the position of the respective surface zones.

Author Manuscript Author Manuscript Author Manuscript Author Manuscript

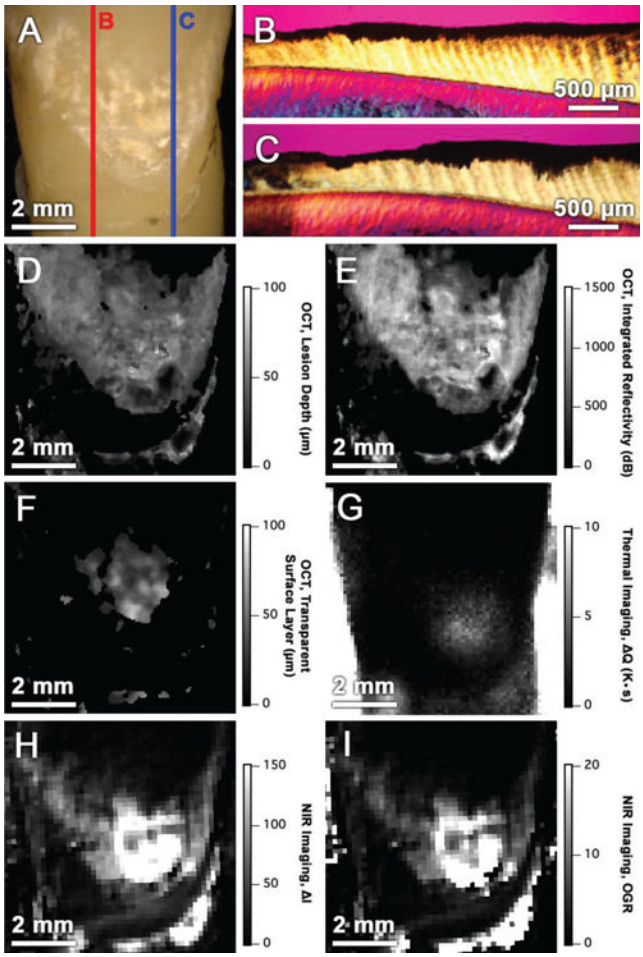

Fig. 2.

Visible, cross-sectional PLM, PS-OCT, thermal, and NIR reflectance images of an active smooth surface enamel caries lesion. The red line in the visible light reflectance image (A) represents the position of the PLM section shown in (B) and the blue line represents the position of the PLM section shown in (C). Lesion depths (D), lesion severity, estimated with integrated reflectivity (E), and transparent surface layer thickness (F) measurements with PS-OCT correlate well with histology (B and C). ΔQ (G) measurements with thermal imaging and ΔI (H) and OGR (I) measurements with NIR imaging show the suspected lesion.

Author Manuscript Author Manuscript Author Manuscript Author Manuscript

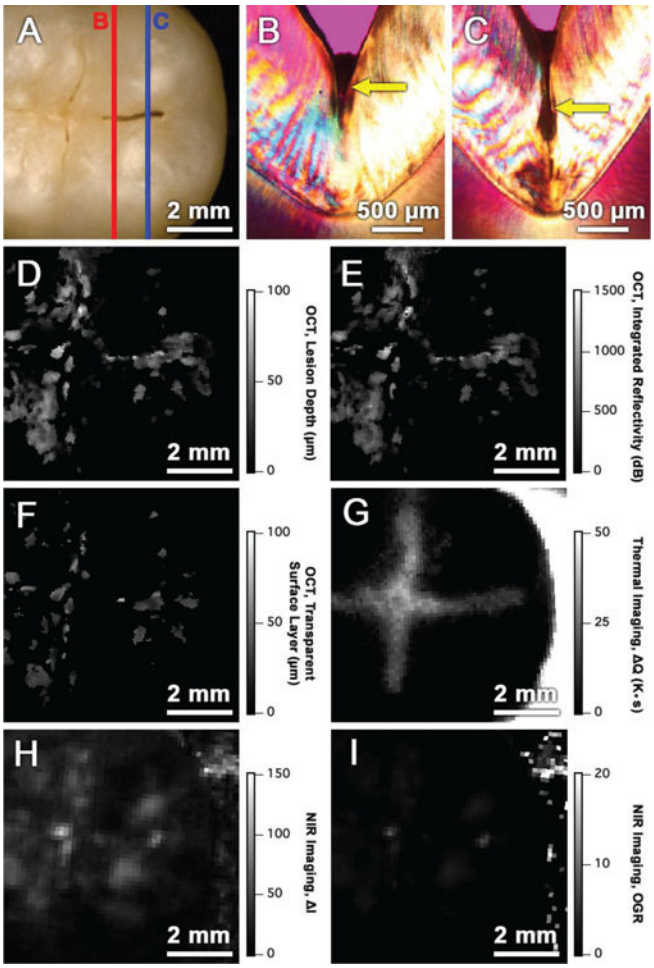

Fig. 3.

Visible, cross-sectional PLM, PS-OCT, thermal, and NIR reflectance images of an arrested occlusal pits and fissure caries lesion. The red line in the visible light reflectance image (A) represents the position of the PLM section shown in (B) and the blue line represents the position of the PLM section shown in (C). Lesion depths (D), lesion severity, estimated with integrated reflectivity (E), and transparent surface layer thickness (F) measurements with PS-OCT correlate well with histology (B and C). ΔQ (G) measurements with thermal imaging and ΔI (H) and OGR (I) measurements with NIR imaging show the suspected lesion. Yellow arrows designate the position of the respective surface zones.

Author Manuscript Author Manuscript Author Manuscript Author Manuscript

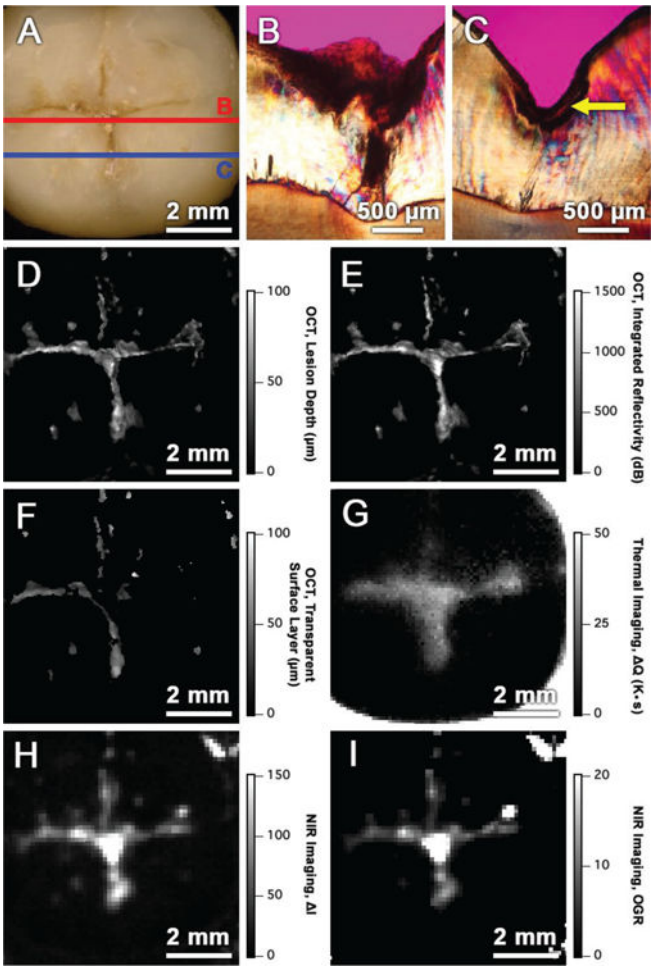

Fig. 4.

Visible, cross-sectional PLM, PS-OCT, thermal, and NIR reflectance images of an active occlusal pits and fissure caries lesion. The red line in the visible light reflectance image (A) represents the position of the PLM section shown in (B) and the blue line represents the position of the PLM section shown in (C). Lesion depths (D), lesion severity, estimated with integrated reflectivity (E), and transparent surface layer thickness (F) measurements with PS-OCT correlate well with histology (B and C). ΔQ (G) measurements with thermal imaging and ΔI (H) and OGR (I) measurements with NIR imaging show the suspected lesion. A yellow arrow designates the position of the respective surface zones.

Author Manuscript Author Manuscript Author Manuscript Author Manuscript

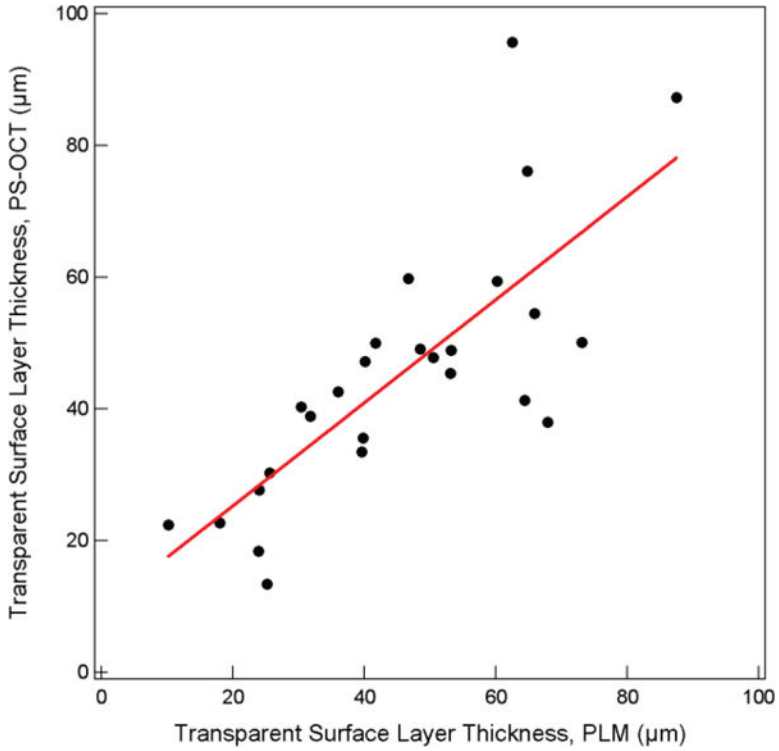

Fig. 5.

A plot of transparent surface layer thickness determined with histology (PLM) vs. thickness estimated from the automated algorithm (PS-OCT). Only the true-negative samples are shown above (n = 26).

Author Manuscript

Author Manuscript

Author Manuscript

Author Manuscript

TABLE I

Mean ± S.D. ΔR, ΔQ, ΔI and OGR measurements

	Smooth Surfaces		Pits and Fissures	
	Active (n = 4)	**Arrested (n = 18)**	**Active (n =10)**	**Arrested (n = 10)**
ΔR (dB×μm)	1276 ± 456 a	1226 ± 445 a	1139 ± 582 a	548 ± 271 b
ΔQ (K×s)	16.9 ± 17.1 a,b	0.9 ± 1.7 c	31.0 ± 15.6 a	7.3 ± 4.2 b,c
ΔI	207 ± 88 a,b	41 ± 28 c	231 ± 205 a	48 ± 28 b,c
OGR	33.3 ± 16.1 a,b	3.4 ± 2.5 c	45.3 ± 38.1 a	6.5 ± 4.4 b,c

Groups with the same letters are statistically similar, P > 0.05 in each row.

Author Manuscript

Author Manuscript

Author Manuscript

Author Manuscript

TABLE II

ROC Curve Analysis of ΔR, ΔQ, ΔI and OGR measurements

	Smooth Surfaces		Pits and Fissures	
	AUC*	**P-value**	**AUC***	**P-value**
ΔR (PS-OCT)	0.51	0.9322	0.84	0.0102
ΔQ (Thermal)	0.97	0.0038	0.95	0.0007
ΔI (NIR)	0.99	0.0029	0.97	0.0004
OGR (NIR)	1.00	0.0022	0.94	0.0009

*AUC represents the area under the curve of the ROC analysis